COMMUNICATIONS CHEMISTRY

ARTICLE

https://doi.org/10.1038/s42004-020-00381-2 OPEN

Enhanced CO evolution for photocatalytic conversion of CO_2 by H_2O over Ca modified Ga_2O_3

Rui Pang[1], Kentaro Teramura[1,2✉], Masashige Morishita[1], Hiroyuki Asakura[1,2], Saburo Hosokawa[1,2] & Tsunehiro Tanaka[1,2✉]

Artificial photosynthesis is a desirable critical technology for the conversion of CO_2 and H_2O, which are abundant raw materials, into fuels and chemical feedstocks. Similar to plant photosynthesis, artificial photosynthesis can produce CO, CH_3OH, CH_4, and preferably higher hydrocarbons from CO_2 using H_2O as an electron donor and solar light. At present, only insufficient amounts of CO_2-reduction products such as CO, CH_3OH, and CH_4 have been obtained using such a photocatalytic and photoelectrochemical conversion process. Here, we demonstrate that photocatalytic CO_2 conversion with a Ag@Cr-decorated mixture of $CaGa_4O_7$-loaded Ga_2O_3 and the CaO photocatalyst leads to a satisfactory CO formation rate (>835 μmol h^{-1}) and excellent selectivity toward CO evolution (95%), with O_2 as the stoichiometric oxidation product of H_2O. Our photocatalytic system can convert CO_2 gas into CO at >1% CO_2 conversion (>11531 ppm CO) at ambient temperatures and pressures.

[1] Department of Molecular Engineering, Graduate School of Engineering, Kyoto University, Kyotodaigaku Katsura, Nishikyo-ku, Kyoto 615-8510, Japan. [2] Element Strategy Initiative for Catalysts & Batteries (ESICB), Kyoto University, 1-30 Goryo-Ohara, Nishikyo-ku, Kyoto 615-8245, Japan. ✉email: teramura@moleng.kyoto-u.ac.jp; tanakat@moleng.kyoto-u.ac.jp

Carbon dioxide (CO_2) concentrations in the atmosphere have increased drastically over the past few centuries owing to the combustion of carbon-rich fossil fuels such as coal, oil, and natural gas. As a major anthropogenic greenhouse gas, these ever-increasing CO_2 emissions are detrimental to the environment and will affect both ecosystems and the global climate[1]. Therefore, there is a critical requirement of mitigating CO_2 emissions to achieve sustainable development. Since the pioneering work on the photocatalytic conversion of CO_2 into formic acid (HCOOH) and methyl alcohol (CH_3OH) over semiconductors reported by Halmann and Inoue et al.[2,3], the photocatalytic conversion of CO_2 into other valuable feedstocks at ambient temperatures and pressures has attracted considerable attention from the scientific community as a feasible strategy for CO_2 storage and conversion[4–8].

In general, the photocatalytic conversion of CO_2 over an excited semiconductor-based catalyst involves three main steps. First, CO_2 molecules are adsorbed on the photocatalyst surface[9–11]. Second, the photogenerated electrons react with the adsorbed CO_2 species and protons (H^+) to yield products such as carbon monoxide (CO), methane (CH_4), CH_3OH, and HCOOH. Among these possible reduction products, CO is one of the most useful because it is widely combined with H_2 to provide synthetic gas for use in many chemical processes, such as methanol synthesis[12,13] and the industrial Fischer–Tropsch process that produce various chemicals and synthetic fuels[14,15]. Third, the products are desorbed from the photocatalyst surface. However, as the H/H_2 redox potential (−0.41 V vs. NHE at pH 7) is more positive than that for CO_2/CO (−0.52 V vs. NHE at pH 7), the generation of H_2 from H^+ is preferable for the photocatalytic conversion of CO_2 into CO, where H_2O acts as the electron donor[16–18]. Moreover, because of the high thermodynamic stability of the linear CO_2 molecule, the fixation and activation of CO_2 are also immense challenges in the photocatalytic conversion of CO_2 by H_2O[4,19]. Thus, although various heterogeneous photocatalysts have been reported for the photocatalytic conversion of CO_2 into CO with H_2O as the electron donor[20–24], the photocatalytic activity for CO evolution remains limited to a few micromoles, while the photocatalytic conversion rate of CO_2 into CO is <0.15%.

Based on the processes involved in the photocatalytic conversion of CO_2 described previously, we deduce that the photocatalytic activity of the photocatalyst for CO_2 conversion can be improved by increasing CO_2 adsorption, charge separation, and product desorption. Due to the fact that CO_2 acts as a Lewis acid that bonds easily with Lewis bases[25], many studies have focused on improving CO_2 adsorption by modifying the photocatalyst surface with a CO_2 adsorbent, such as NaOH[26], amino groups[27], and rare earth species[28], to increase the photocatalytic activity and selectivity for CO_2 conversion by H_2O. Our group reported that modifying the photocatalyst surface with alkaline earth metals (e.g., Ca, Sr, and Ba) enhanced the conversion of CO_2 and the selectivity toward CO evolution[29]. Moreover, we found that a Ag@Cr core/shell cocatalyst suppresses the backward reaction from CO and O_2 to CO_2, and enhances the adsorption of CO_2, resulting in a highly selective photocatalytic CO_2 conversion[30,31].

In this study, we exploited the above techniques and successfully fabricated a Ag@Cr-decorated mixture of $CaGa_4O_7$-loaded Ga_2O_3 and CaO photocatalyst, which exhibits a high CO formation rate (>835 μmol h^{-1}) per 0.5 g of catalyst, in addition to high selectivity toward CO evolution (>95%) with the stoichiometric production of O_2 as the oxidation product of H_2O during the photocatalytic conversion of CO_2 by H_2O. Approximately 1.2% of the CO_2 in the gas phase was transformed into CO (11531 ppm) as a product. The results reported in this study represent almost an order of magnitude higher than most previously published results, as summarized in Supplementary Table 1.

Results and discussion

Photocatalytic reduction of CO_2 by H_2O. Table 1 shows the formation rates of CO, H_2, and O_2, selectivity toward CO evolution, and the balance between consumed electrons and holes over the bare Ga_2O_3, Ag-modified Ga_2O_3 (Ag/Ga_2O_3), Ag@Cr-modified Ga_2O_3 ($Ag@Cr/Ga_2O_3$), and Ag@Cr-modified Ca-loaded Ga_2O_3 ($Ag@Cr/Ga_2O_3$_Ca) photocatalysts during the photocatalytic conversion of CO_2 by H_2O. No liquid products were detected in the reaction solutions in these photocatalytic systems, and H_2, O_2, and CO were detected as gaseous products. As no reduction products other than H_2 and CO were generated, the selectivity toward CO evolution and the balance between the consumed electrons and holes were calculated as follows:

$$\text{Selectivity toward CO evolution}\,(\%) = 2R_{CO}/(2R_{CO} + 2R_{H2}) \times 100, \quad (1)$$

$$\text{Consumed}\, e^-/h^+ = (2R_{CO} + 2R_{H2})/4R_{O2}, \quad (2)$$

where R_{CO} and R_{H2} represent the formation rates of CO and H_2, respectively. If H_2O acts as an electron donor, the value of e^-/h^+ should be equal to 1.

We obtained stoichiometric amounts of H_2 and CO as reduction products in addition to O_2 as the oxidation product, indicating that H_2O serves as the electron donor. Bare Ga_2O_3 exhibited a particularly low selectivity toward CO evolution (4%) as the electrons generated by charge transfer were not consumed in the reduction of CO_2, but rather in the production of H_2 from H^+. Modifying Ga_2O_3 with a Ag cocatalyst enhanced the selectivity toward CO evolution (29%); however, this was not sufficient to obtain a selectivity >50%. In contrast, we succeeded in the selective photocatalytic conversion of CO_2 by H_2O over $Ag@Cr/Ga_2O_3$. A relatively high CO formation rate (499.6 μmol h^{-1}) was achieved with 77% selectivity toward CO evolution. The photocatalytic reaction for the conversion of CO_2 by H_2O over $Ag@Cr/Ga_2O_3$ and $Ag@Cr/Ga_2O_3$_Ca was

Table 1 Photocatalytic conversions of CO_2 by H_2O using various photocatalysts.

Catalyst	Formation rates of products (μmol h^{-1})			Selec. toward CO (%)	Consumed e^-/h^+
	H_2	O_2	CO		
Bare Ga_2O_3	240.9	122.8	9.8	4	1.02
Ag/Ga_2O_3	248.3	172.7	102.1	29	1.01
$Ag@Cr/Ga_2O_3$	148.5	316.4	499.6	77	1.02
$Ag@Cr/Ga_2O_3$_Ca	176.5	448.2	794.2	82	1.08

Photocatalyst powder: 0.5 g, reaction solution volume: 1.0 L, additive: 0.1 M $NaHCO_3$, CO_2 flow rate: 30 mL min^{-1}, light source: 400-W high-pressure Hg lamp.

carried out for at least four times, and errors in the product formation rates (H_2, O_2, and CO) were smaller than 5%. Controlling both, the bulk and surface of the photocatalysts, is highly important for achieving a considerably high CO formation rate and selectivity toward CO evolution. We found that the amount of Ca species significantly affected the H_2 and CO formation rates (for the product formation rates and selectivity over various Ag@Cr/Ga_2O_3_Ca photocatalysts see Supplementary Fig. 1). The formation rate of CO increased first and then decreased as the Ca content increased (Supplementary Fig. 1a–g). In contrast, the formation rate of H_2 over the Ag–Cr/Ga_2O_3_Ca_x samples increased monotonically with increasing amount of Ca species. The Ag–Cr/$CaGa_4O_7$ photocatalyst was only active for H_2 evolution derived from water splitting (Supplementary Fig. 1h). The Ag@Cr/Ga_2O_3_Ca photocatalyst exhibited the highest CO formation rate (794.2 μmol h^{-1}), and the selectivity toward CO evolution was approximately 82%. Additionally, CO production from the photocatalytic conversion of CO_2 after photoirradiation for 15 h over Ag@Cr/Ga_2O_3_Ca was more stable than that over Ag@Cr/Ga_2O_3 (for the product formation rates for 15 h see Supplementary Fig. 2), which indicates that the presence of Ca species is not only beneficial for improving the photocatalytic activity and selectivity, but also for improving stability during the photocatalytic conversion of CO_2 to CO.

Various control experiments were carried out to confirm the source of CO during the photocatalytic conversion of CO_2 by H_2O, the results of which are shown in Supplementary Fig. 3. We did not detect any appreciable amounts of products under dark conditions or in the absence of a photocatalyst. In addition, H_2 was the main product formed when Ar gas was used instead of CO_2 or in the absence of $NaHCO_3$. The control experiments confirmed that the evolved CO originated from the CO_2 gas introduced into the samples and not from carbon contaminants.

Photocatalyst characterization. The actual amounts of the Ca species loaded into Ga_2O_3 at different $CaCl_2$ concentrations were measured using inductively coupled plasma optical emission spectrometry (ICP-OES) (Supplementary Table 2). We found that almost all the Ca species were loaded into the Ga_2O_3 photocatalyst when the $CaCl_2$ concentration was <0.001 mol L^{-1}. However, not all the Ca species could be loaded into Ga_2O_3 at higher $CaCl_2$ concentrations. Note that even when no $CaCl_2$ was added during the preparation of Ga_2O_3, trace amounts of Ca were detected in Ga_2O_3, which is likely due to Ca impurities present in the experimental vessels or precursor reagents. Hereinafter, we refer to the Ca-loaded Ga_2O_3 photocatalysts as Ga_2O_3_Ca_x (x = 0.32, 0.62, 1.1, 1.6, 2.1, 3.3 mol%) based on the Ca/Ga molar ratio determined by ICP-OES. Figure 1a shows the X-ray diffraction (XRD) patterns of the bare Ga_2O_3, Ga_2O_3_Ca_x, and $CaGa_4O_7$ photocatalysts. As indicated, gradual changes in the diffraction peaks assigned to the (020), (311), (400), (002), and (330) facets of $CaGa_4O_7$ (JSPDS 01-071-1613) were observed as the amount of Ca species was increased. In general, a high Ca loading is favorable for the formation of $CaGa_4O_7$. We observed no distinct shifts in the diffraction peaks for the Ga_2O_3_Ca_x samples compared with those of bare Ga_2O_3. As the ionic radius of Ca^{2+} (0.099 nm)[32] is larger than that of Ga^{3+} (0.062 nm)[33], the unshifted XRD peaks imply that Ca^{2+} does not act as a dopant in the bulk Ga_2O_3 lattice. However, there was a clear increase in the peak intensity at $2\theta = 30.1°$ and an apparent decrease in that at $2\theta = 30.5°$ with increasing amount of Ca species (Fig. 1b), which are possibly ascribed to the formation of $CaGa_4O_7$ species on Ga_2O_3. The increased intensity of the Ca 2p X-ray photoelectron spectroscopy (XPS) peak (Fig. 1c) also indicates that the amount of Ca species on the Ga_2O_3 surface increased with increasing Ca levels. In addition, the XPS peak locations in the Ca 2p spectra of the Ga_2O_3_Ca_x photocatalysts are similar to those of $CaGa_4O_7$, but different from those of CaO. The Ca 2p XPS profiles suggest that a thin $CaGa_4O_7$ layer forms on the Ga_2O_3 surface and that the amount of $CaGa_4O_7$ increases as the amount of Ca is increased. We further confirmed the morphological changes in the Ga_2O_3_Ca sample by field-emission scanning electron microscopy (SEM), as shown in Fig. 1d. Both ends of the Ga_2O_3 nanoparticles gradually sharpened and their surfaces became smoother as the amount of Ca species increased, especially when the Ca amount was higher than 1.1 mol%. This smoothing of the Ga_2O_3 surfaces with increasing Ca/Ga molar ratio resulted in a decrease in the Brunauer–Emmett–Teller (BET) specific surface area of Ga_2O_3_Ca_x (Supplementary Fig. 4), which is attributable to the modification of $CaGa_4O_7$, as we confirmed from the XRD patterns and the XPS results that a $CaGa_4O_7$ layer was formed on the Ga_2O_3 surface.

The close linkage between $CaGa_4O_7$ and Ga_2O_3 on the Ga_2O_3 surface was confirmed by field-emission transmission electron microscopy (TEM) and high-resolution TEM (HRTEM) (Fig. 2). The marked lattice spacings (0.296 and 0.255 nm) in Fig. 2b correspond to the (130) and (111) planes of $CaGa_4O_7$ and Ga_2O_3, respectively. The core–shell-structured Ag@Cr cocatalyst was successfully loaded onto the Ga_2O_3_Ca surface using the photodeposition method (Fig. 2c, d), as reported previously by us[31].

Role of the Ca species. Figure 3 shows the Fourier transform infrared (FTIR) spectra of the CO_2-adsorbed samples after introducing CO_2 at ~0.2 Torr. When CO_2 was introduced into the Ga_2O_3 sample, three absorbance peaks were observed at 1634, 1432, and 1225 cm^{-1}, which can be ascribed to asymmetric CO_3 stretching vibrations [$\nu_{as}(CO_3)$], symmetric CO_3 stretching vibrations [$\nu_s(CO_3)$] of monodentate bicarbonate species (m-HCO_3-Ga), and OH deformation vibrations [δ(OH)], respectively[34–36]. The absorbance peaks at 1699 and 1636 cm^{-1} for the CO_2-adsorbed CaO sample can be attributed to bridging carbonate stretching and asymmetric CO_3 stretching vibrations [$\nu_{as}(CO_3)$] of the bicarbonate species, respectively. The broad structureless absorbance peaks between 1480 and 1318 cm^{-1} can be attributed to the symmetric and asymmetric CO_3 stretching of unidentate carbonate, as well as the symmetric CO_3 stretching [$\nu_s(CO_3)$] of bicarbonate[37–41]. When the Ga_2O_3 surface was modified with a small amount of Ca species, absorbance peaks attributable to CO_2 adsorption by both Ga_2O_3 and CaO were observed after CO_2 was introduced into the Ga_2O_3_Ca_1.1 sample. However, when the Ga_2O_3 surface was modified with large amounts of Ca species, the absorbance peaks attributed to CO_2 adsorption on Ga_2O_3 had low intensity and mainly corresponded to the broad peaks derived from the adsorption of CO_2 on $CaGa_4O_7$. Supplementary Fig. 5 shows the FTIR spectra of CO_2-adsorbed Ga_2O_3, Ga_2O_3_Ca_1.1, Ga_2O_3_Ca_3.3, and $CaGa_4O_7$ samples after introducing the same amount of CO_2 at various pressures in the 0.1–40.0 Torr range. CO_2 was adsorbed significantly more on the Ga_2O_3_Ca_1.1 surface than on the Ga_2O_3 surface due to its adsorption at both Ga and Ca sites. However, the $CaGa_4O_7$ surface was not conducive to CO_2 adsorption; therefore, CO_2 adsorbed less onto the Ga_2O_3_Ca_3.3 surface than the Ga_2O_3_Ca_1.1 surface.

Figure 4 shows the FTIR spectra of the adsorbed CO_2 species on Ga_2O_3_Ca_1.1 after different durations of photoirradiation. As the photoirradiation time increased from 0 to 106 h, the bands at 1225 [δ(OH)-Ga] and 1408 cm^{-1} [$\nu_s(CO_3)$-Ca] decreased and

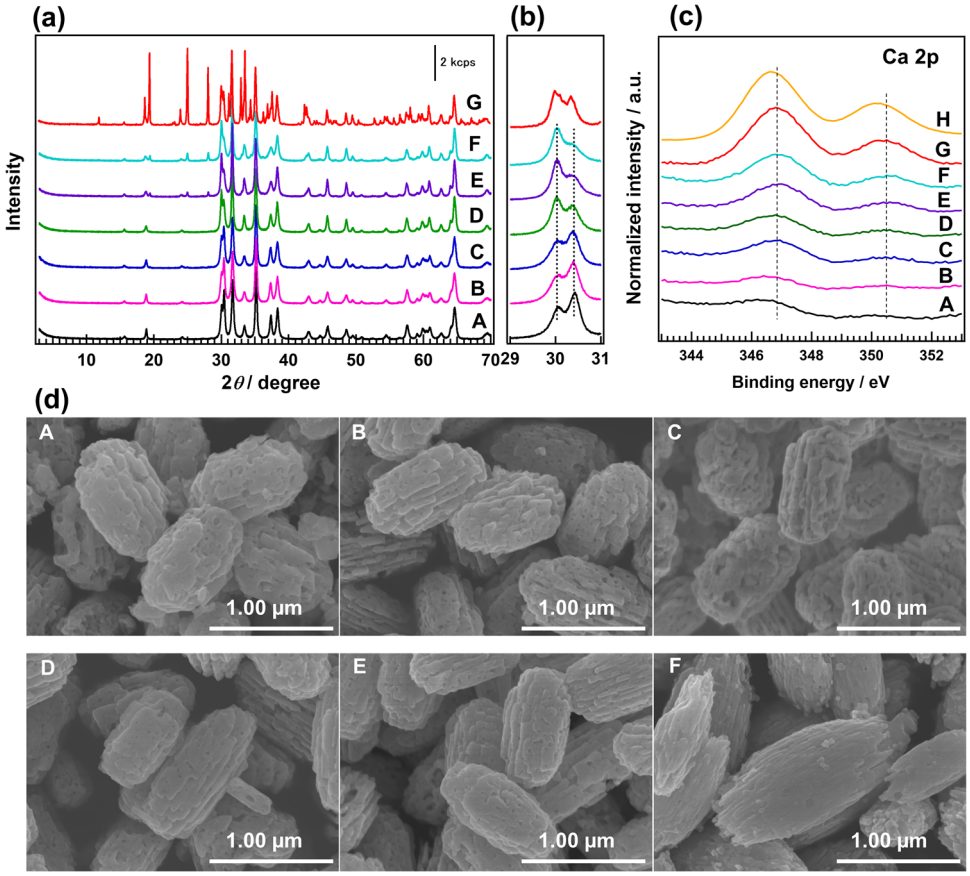

Fig. 1 Photocatalyst characterization. a X-ray diffractograms; **b** enlarged X-ray diffractograms at $2\theta = 29$–$31°$; **c** Ca 2p X-ray photoelectron spectroscopy profiles; and **d** field-emission scanning electron microscopy images of **A** bare Ga_2O_3; Ga_2O_3_Ca_x with a Ca/Ga molar ratio x of **B** 0.32 mol%, **C** 0.62 mol%, **D** 1.1 mol%, **E** 2.1 mol%, and **F** 3.3 mol%; **G** $CaGa_4O_7$ (in **a**, **b**), and **H** CaO (in **c**).

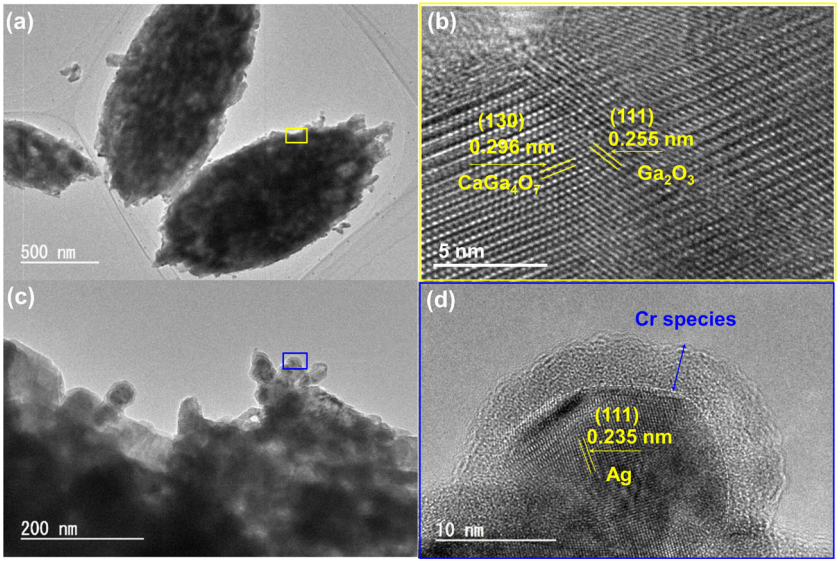

Fig. 2 Transmission electron microscopy (TEM) images of the photocatalysts. TEM images of **a** Ga_2O_3_Ca and **c** Ag@Cr/Ga_2O_3_Ca. High-resolution TEM images of **b** Ga_2O_3_Ca and **d** Ag@Cr/Ga_2O_3_Ca. Note that **b**, **d** are enlarged TEM images of the marked areas in **a**, **c** indicated by yellow and blue boxes, respectively.

vanished after 104 h. At the same time, new bands gradually appeared at 1581, 1388, and 1353 cm^{-1} (asymmetric CO_2 stretching [$\nu_{as}(CO_2)$], CH deformation [δ(CH)], and symmetric CO_2 stretching [$\nu_s(CO_2)$] assigned to formate species (HCOO–Ga/Ca), respectively)[34–36]. As the photoirradiation continued, the formate species were consumed and gaseous CO (fundamental vibration band at 2143 cm^{-1})[42] was formed simultaneously. This result indicates that the bicarbonate species is the intermediate during the photocatalytic conversion of CO_2, and the formates transform into CO with photoirradiation, which

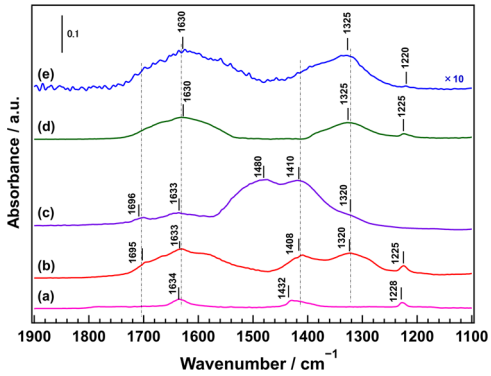

Fig. 3 Fourier transform infrared spectra of CO_2 adsorption. CO_2 adsorbed on: **a** Ga_2O_3, **b** Ga_2O_3_Ca_1.1, **c** CaO, **d** Ga_2O_3_Ca_3.3, and **e** $CaGa_4O_7$ after introducing ~0.2 Torr of CO_2.

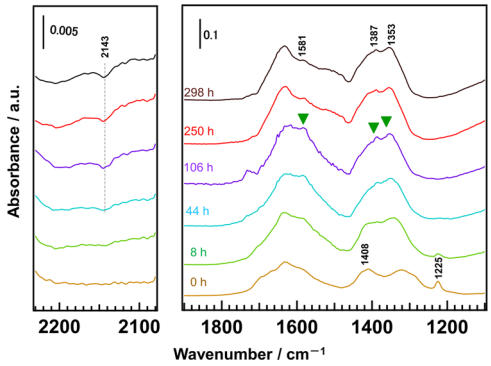

Fig. 4 FTIR spectra of CO_2 adsorption under photoirradiation. Difference FTIR spectra of the adsorbed CO_2 species on Ga_2O_3_Ca_1.1 under photoirradiation for different hours. ~2.0 Torr of CO_2 was introduced into the instrument.

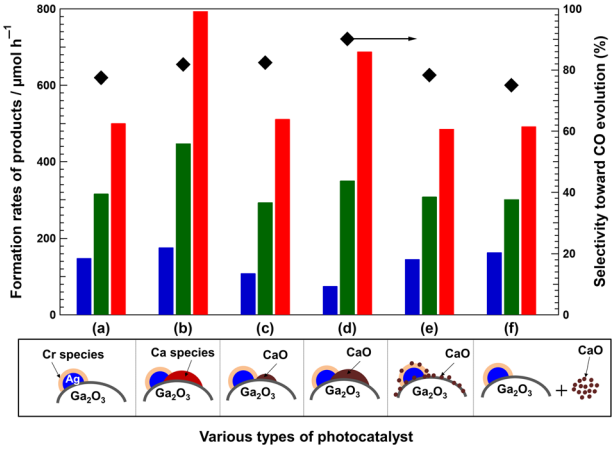

Fig. 5 Product formation rates and selectivity. Rates of formation of H_2 (blue bars), O_2 (green bars), and CO (red bars), as well as selectivity toward CO evolution (black diamonds) for various photocatalysts: **a** Ag@Cr/Ga_2O_3; **b** Ag@Cr/Ga_2O_3_Ca_1.1; **c** Ag@Cr/(1.1 mol%CaO/Ga_2O_3), namely Ga_2O_3 physically mixed with 1.1 mol% of CaO by grinding before loading the Ag@Cr cocatalyst; **d** Ag@Cr/(30 mol%CaO/Ga_2O_3), which is similar to **c** except for using 30 mol% of CaO; **e** Ag@Cr/Ga_2O_3 + 30 mol% CaO, namely Ag@Cr/Ga_2O_3 physically mixed with 30 mol% of CaO by grinding; and **f** Ag@Cr/Ga_2O_3 and 30 mol% of CaO without mixing before adding into the reaction solution. Schematic structures of the photocatalysts are shown at bottom. Photocatalyst powder: 0.5 g, reaction solution volume: 1.0 L, additive: 0.1 M $NaHCO_3$, CO_2 flow rate: 30 mL min^{-1}, light source: 400 W high-pressure Hg lamp.

is consistent with our previous results[43,44]. It is worth mentioning that in addition to the presence of intermediate species on the Ga_2O_3 surface ([δ(OH)–Ga]), the modification by Ca species further increased the amount of intermediate on Ga_2O_3_Ca_1.1. As the photocatalytic conversion of H^+ into H_2 and the conversion of CO_2 into CO are two competing processes in an aqueous solution, the high adsorption of CO_2 at the base site leads to high photocatalytic activity and selectivity toward CO evolution during the photocatalytic conversion of CO_2 by H_2O.

In order to demonstrate that the presence of CaO on the Ga_2O_3 surface enhances the photocatalytic activity and selectivity during the photocatalytic conversion of CO_2 into CO, we investigated the photocatalytic performance during the conversion of CO_2 by H_2O over various Ag@Cr/CaO/Ga_2O_3 photocatalysts, the results of which are shown in Fig. 5. We found that the Ag@Cr/Ga_2O_3_Ca_1.1 photocatalyst (with a low amount of CaO generated on the Ga_2O_3 surface) significantly enhanced the rate of CO formation during the photocatalytic conversion of CO_2 by H_2O compared with bare Ag@Cr/Ga_2O_3 (Fig. 5a, b). However, no significant change in the rate of CO formation and selectivity toward CO evolution was observed for the sample labeled "Ag@Cr/(1.1 mol%CaO/Ga_2O_3)" (in which 1.1 mol% CaO was physically loaded onto Ga_2O_3 by grinding before loading Ag@Cr cocatalyst onto the CaO/Ga_2O_3 surface) as compared to bare Ga_2O_3 (Fig. 5c). Because uncalcined CaO-loaded Ga_2O_3 easily dissolves in H_2O, we increased the CaO loading on the Ga_2O_3 surface to 30 mol% using the same grinding method (labeled "Ag@Cr/(30 mol%CaO/Ga_2O_3)"), which resulted in an increased rate of CO formation and a decrease in H_2 formation (Fig. 5d). However, no improvement in photocatalytic activity and selectivity was observed when 30 mol% CaO was mixed with the prepared Ag@Cr/Ga_2O_3 and ground together (Fig. 5e) or when they were directly mixed in the reaction solution (Fig. 5f). These results clearly reveal that the addition of CaO on the Ga_2O_3 surface enhances the rate of CO formation and suppresses that of H_2 during the photocatalytic conversion of CO_2 by H_2O. In addition, the tight junction between Ga_2O_3, CaO, and the Ag@Cr cocatalyst is crucial for the superior photocatalytic activity and selectivity of the photocatalyst for the conversion of CO_2 into CO. In our previous work, we confirmed that Ag acts as an active site while the $Cr(OH)_3{\cdot}H_2O$ layer exterior to the Ag core increases CO_2 adsorption[30,31]. Hence, the Ag@Cr cocatalyst should be loaded at the CaO/Ga_2O_3 interface in order to facilitate contact between the CaO-adsorbed CO_2 species and the Ag active sites.

Notably, although $CaGa_4O_7$ exhibited high selectivity toward H_2 evolution, the H_2 formation rate for $CaGa_4O_7$ was significantly lower than that for Ga_2O_3_Ca_3.3 (for the product formation rates over Ag-Cr/Ga_2O_3_Ca_3.3 see Supplementary Fig. 6). This indicates that the presence of $CaGa_4O_7$ on the Ga_2O_3 surface enhances the overall photocatalytic efficiency during the photocatalytic reaction, including CO_2 conversion and water splitting. The Mott–Schottky plot (Supplementary Fig. 7) and the absorption spectra converted from the diffuse reflectance spectra using the Kubelka–Munk equation (Supplementary Fig. 8) enabled us to estimate the conduction band (CB) and valence band (VB) positions of Ga_2O_3, Ga_2O_3_Ca_0.62, and $CaGa_2O_7$, as shown in Supplementary Fig. 9. Since the CB and VB of Ga_2O_3 are both more positive than those of $CaGa_4O_7$, a heterojunction system between Ga_2O_3 and $CaGa_4O_7$ can be formed that greatly improves the spatial separation efficiency of the photogenerated carriers[45]. Therefore, $CaGa_4O_7$/Ga_2O_3 exhibited a much higher photocatalytic efficiency than bare Ga_2O_3 and $CaGa_4O_7$.

We expect that by exploiting the high CO_2 adsorption of CaO and the high photocatalytic efficiency of $CaGa_4O_7$/Ga_2O_3, we can

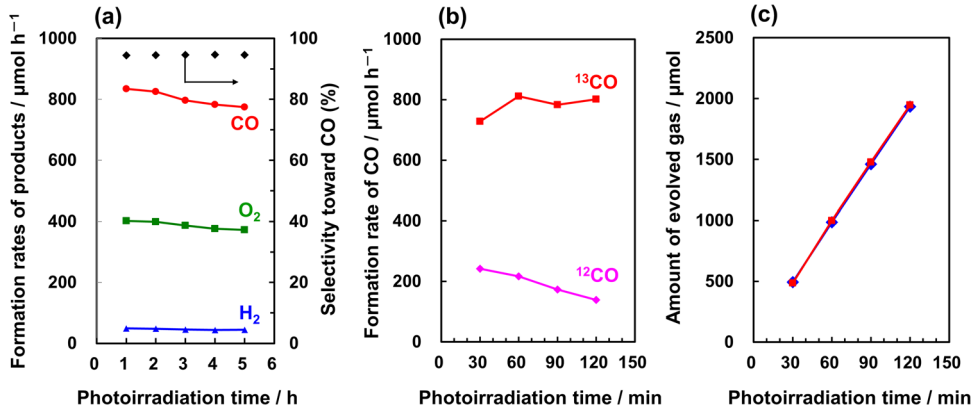

Fig. 6 CO, O_2, and H_2 formation data. a Formation rates of H_2 (blue triangles), O_2 (green squares), and CO (red circles), and selectivity toward CO evolution (black diamonds) for the photocatalytic conversion of CO_2 by H_2O; **b** ^{12}CO and ^{13}CO detected by MS ($m/z = 28$ and 29) from the photocatalytic conversion of $^{13}CO_2$ by H_2O; **c** CO time-course as determined by MS (red squares) and GC (blue diamonds) for the photocatalytic conversion of $^{13}CO_2$ by H_2O.

further improve the photocatalytic activity and selectivity of the photocatalyst to maximize the conversion of CO_2 into CO by H_2O. Figure 6a shows the formation rates of H_2, O_2, and CO during the photocatalytic conversion of CO_2 by H_2O for the Ga_2O_3_Ca_3.3 photocatalyst physically mixed with 30 mol% of CaO and Ag@Cr as the cocatalyst. As indicated, a high formation rate of CO (>835 μmol h^{-1}) was achieved, in addition to an excellent selectivity toward CO evolution (>95%), with a stoichiometric amount of evolved O_2. Both ^{12}CO and ^{13}CO were detected using quadrupole mass spectrometry (MS), and the peaks at $m/z = 28$ and $m/z = 29$ were located at the same positions as those detected by gas chromatography (GC) during the photocatalytic conversion of $^{13}CO_2$ (for the isotopic lead experiments see Supplementary Fig. 10). Indeed, our results indicate that the detected ^{12}CO was produced from the reduction of $^{12}CO_2$ derived from the $NaHCO_3$ additive in the solution[43]. As shown in Fig. 6b, with the consumption of $^{12}CO_2$ derived from $NaHCO_3$, the amount of generated ^{12}CO gradually decreased, while the ^{13}CO content increased under continuous bubbling of $^{13}CO_2$. The total amounts of ^{13}CO and ^{12}CO detected by MS were consistent with the amount of CO detected by GC (Fig. 6c), which indicates that the CO was generated as the reduction product of either CO_2 introduced in the gas phase or from $NaHCO_3$, rather than from any organic contaminants on the photocatalyst surface. The converted concentration of CO based on the CO formation rate was found to be 11,531 ppm, indicating that ~1.2% of CO_2 in the gas phase was transformed into CO (see Supplementary Information for the calculation details. The actual amounts of CO detected are shown in Supplementary Movie 1).

In our previous work, we had found that basic oxides and hydroxides such as $Cr(OH)_3$[31], SrO[44], and rare earth (RE) hydrates and oxides[28] function as good CO_2 storage materials by generating the corresponding (hydroxy)carbonate compounds (e.g., $Cr(OH)_x(CO_3)_y$ and $RE_2(OH)_{2(3-x)}(CO_3)_x$), and they improve the photocatalytic activity and selectivity toward CO evolution. Now, we propose a possible mechanism for the photocatalytic conversion of CO_2 by H_2O over Ag@Cr/CaO/$CaGa_2O_7/Ga_2O_3$, as shown in Fig. 7. During the photocatalytic conversion of CO_2 in an aqueous solution of $NaHCO_3$, the Cr $(OH)_3{\cdot}H_2O$ and CaO species that are in close contact with Ag particles easily form (hydroxy)carbonate species (named M $(OH)_x(CO_3)_y$, M=Cr or Ca)[31], which greatly increase the concentration of CO_2-related species around the Ag active sites, thereby improving selectivity for the photocatalytic conversion of CO_2 into CO instead of water splitting. On the other hand, the $Ga_2O_3/CaGa_4O_7$ heterojunction improves the efficiency for

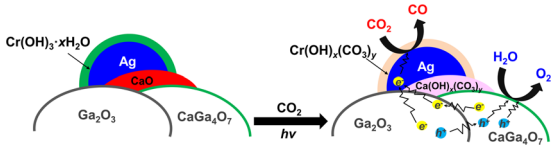

Fig. 7 A plausible reaction mechanism. Schematic illustration of the mechanism for the photocatalytic conversion of CO_2 into CO over Ag@Cr/CaO/$CaGa_4O_7/Ga_2O_3$.

spatial separation of the photogenerated carriers, which also increases the photocatalytic activity for the conversion of CO_2 into CO. Moreover, while the $Cr(OH)_3{\cdot}xH_2O$ shell outside the Ag particle can be oxidized to Cr^{6+} and dissolve into the solution during the photocatalytic conversion of CO_2[46], the presence of CaO around the Ag active site compensates for the reduced activity from the dissolution of Cr species. As a result, Ag@Cr/Ga_2O_3_Ca is photocatalytically much more stable than Ag@Cr/Ga_2O_3.

Herein, we reported the photocatalytic conversion of CO_2 using a Ag@Cr/CaO/$CaGa_4O_7/Ga_2O_3$ photocatalyst, in which a satisfactory CO formation rate (>835 μmol h^{-1}) and an excellent selectivity toward CO evolution (95%) were achieved with the stoichiometric production of O_2 as the oxidation product of H_2O. Through the use of various characterization techniques, we found that the CaO and $CaGa_4O_7$ formed on the Ga_2O_3 surface improved the adsorption of CO_2 at basic sites in addition to enhancing the total photocatalytic efficiency. In addition, the physical mixing of $CaGa_4O_7/Ga_2O_3$ with CaO was a particularly simple and convenient technique for exploiting the high CO_2 adsorption ability of CaO and the high photocatalytic efficiency of $CaGa_4O_7/Ga_2O_3$. These results are of particular interest, considering that previously, only insufficient amounts of CO_2 reduction products were produced during artificial photosynthesis.

Methods

Ca-modified Ga_2O_3 (Ga_2O_3_Ca) was prepared using the ammonia precipitation method reported by Sakata et al.[47]. In this method, $Ga(NO_3)_3{\cdot}nH_2O$ (12.6 g) was dissolved in 200 mL of deionized water or $CaCl_2$ solution in ultrapure water at various concentrations. Hydroxylation was carried out by dripping an ammonium hydroxide solution until the pH level reached 9.1. The obtained hydroxides were centrifuged and dried overnight. The Ga_2O_3_Ca sample was obtained by calcining the precursor at 1273 K for 10 h. Ag@Cr/Ga_2O_3_Ca was synthesized using the photodeposition method reported in our previous work[30]. In this method, the as-prepared Ga_2O_3_Ca powder (1.0 g) was dispersed in ultrapure water (1.0 L) containing the necessary amounts of silver nitrate ($AgNO_3$) and chromium (III) nitrate

($Cr(NO_3)_3$). The suspension was purged with Ar gas and irradiated under a 400 W high-pressure Hg lamp with Ar gas flowing for 1.0 h, followed by filtration and drying at room temperature (~298 K). The Ag/Ga and Cr/Ga molar ratios were both 1.0 mol%.

Characterization. The as-prepared Ga_2O_3_Ca samples were characterized using the following techniques: XRD (Model: Multiflex, Rigaku Corporation, Japan) with Cu Kα radiation ($\lambda = 0.154$ nm); XPS (Model: ESCA 3400, Shimadzu Corporation, Japan) with Mg Kα radiation; SEM (Model: SU-8220, Hitachi High-Technologies Corporation, Japan); TEM (Model: JEM-2100F, JEOL Ltd, Japan); and UV–Visible spectroscopy (V-650, JASCO) with an integrated sphere accessory. The BET surface areas of the photocatalyst samples were determined from their N_2-adsorption isotherms at 77 K using a volumetric gas-adsorption measuring instrument (Model: BELSORP-miniII, MicrotracBEL Corp. (formerly BEL Japan, Inc.), Japan). Prior to these measurements, each sample was evacuated at 473 K for 1 h using a sample pretreatment system (Model: BELPREP-vacII, MicrotracBEL Corp. (formerly BEL Japan, Inc.), Japan). ICP-OES (Model: iCAP7400, Thermo Fisher Scientific, USA) was used to determine the actual amounts of Ca modified on the Ga_2O_3 surface. The FTIR spectra of the adsorbed carbon species were recorded using an FTIR spectrometer (Model: FT/IR-4700, JASCO International Co., Ltd., Japan) equipped with a mercury–cadmium–tellurium (MCT) detector and cooled with liquid N_2 in the transmission mode at 303 K. Each sample (~30 mg) was pressed into a wafer (diameter: 10 mm) and introduced into the instrument in a cylindrical glass cell with calcium fluoride (CaF_2) windows. The wafer was evacuated at 673 K for 30 min before being examined, followed by treatment with O_2 at ~40 Torr for 30 min, after which the wafer was evacuated for 30 min and cooled to 303 K. The data for each FTIR spectrum were obtained from 128 scans with a resolution of 4 cm^{-1}. The energy gap of the band structure and flat band potential of the Ga_2O_3_Ca samples were determined using the Davis–Mott and Mott–Schottky equations, respectively; the experimental details are provided in the Supplementary Information.

Photocatalytic reaction. The photocatalytic reduction of CO_2 was carried out using a flow system with an inner irradiation-type reaction vessel. The synthesized photocatalyst (0.5 g) was dispersed in ultrapure water (1.0 L) containing 0.1 M sodium bicarbonate ($NaHCO_3$). The CO_2 was bubbled into the solution at a flow rate of 30 mL min^{-1}. The suspension was illuminated using a 400 W high-pressure Hg lamp with a quartz filter, and the assembly was connected to a water-cooling system. The amounts of evolved H_2 and O_2 were detected using a gas chromatography system fitted with a thermal conductivity detector (TCD-GC, Model: GC-8A, Shimadzu Corporation, Japan) and a 5A molecular sieve (MS 5A) column, and Ar was used as the carrier gas. The amount of evolved CO was analyzed using a gas chromatography system fitted with a flame ionization detector (FID-GC, Model: GC-8A, Shimadzu Corporation, Japan), a methanizer, and a ShinCarbon ST column, and N_2 was used as the carrier gas. High-performance liquid chromatography (Model: LC-4000, JASCO, USA) was used to detect the presence of liquid products.

In the isotope experiment, $^{12}CO_2$ was replaced by $^{13}CO_2$. The formation rates of H_2, O_2, ^{12}CO, and ^{13}CO under photoirradiation were detected using a quadrupole mass spectrometer (BELMASS, Microtrac BEL) combined with a TCD-GC detector.

Data availability

The datasets generated during and/or analysed during the current study are available in the [figshare] repository, [https://figshare.com/s/84a5d675a273e507fb55 and/or https://doi.org/10.6084/m9.figshare.12927422].

Received: 9 February 2020; Accepted: 16 September 2020;
Published online: 09 October 2020

References

1. IPCC; Pachauri, R. K. & Meyer, L. A., eds. *Climate Change 2014: Synthesis Report. Contribution of Working Groups I, II and III to the Fifth Assessment Report of the Intergovernmental Panel on Climate Change*. (IPCC, Geneva, 2014).
2. Halmann, M. Photoelectrochemical reduction of aqueous carbon dioxide on p-type gallium phosphide in liquid junction solar cells. *Nature* **275**, 115–116 (1978).
3. Inoue, T., Fujishima, A., Konishi, S. & Honda, K. Photoelectrocatalytic reduction of carbon dioxide in aqueous suspensions of semiconductor powders. *Nature* **277**, 637–638 (1979).
4. Li, K., Peng, B. & Peng, T. Recent advances in heterogeneous photocatalytic CO_2 conversion to solar fuels. *ACS Catal.* **6**, 7485–7527 (2016).
5. Mikkelsen, M., Jørgensen, M. & Krebs, F. C. The teraton challenge. A review of fixation and transformation of carbon dioxide. *Energy Environ. Sci.* **3**, 43–81 (2010).
6. Barber, J. Photosynthetic energy conversion: natural and artificial. *Chem. Soc. Rev.* **38**, 185–196 (2009).
7. Cokoja, M., Bruckmeier, C., Rieger, B., Herrmann, W. A. & Kühn, F. E. Transformation of carbon dioxide with homogeneous transition-metal catalysts: a molecular solution to a global challenge? *Angew. Chem. Int. Ed.* **50**, 8510–8537 (2011).
8. Wu, L. Y. et al. Encapsulating perovskite quantum dots in iron-based metal–organic frameworks (MOFs) for efficient photocatalytic CO_2 reduction. *Angew. Chem. Int. Ed.* **58**, 9491–9495 (2019).
9. Tu, W., Zhou, Y. & Zou, Z. Photocatalytic conversion of CO_2 into renewable hydrocarbon fuels: state-of-the-art accomplishment, challenges, and prospects. *Adv. Mater.* **26**, 4607–4626 (2014).
10. Linsebigler, A. L., Lu, G. & Yates, J. T. Jr Photocatalysis on TiO_2 surfaces: principles, mechanisms, and selected results. *Chem. Rev.* **95**, 735–758 (1995).
11. Vu, N.-N., Kaliaguine, S. & Do, T.-O. Critical aspects and recent advances in structural engineering of photocatalysts for sunlight-driven photocatalytic reduction of CO_2 into fuels. *Adv. Funct. Mater.* **29**, 1901825 (2019).
12. Stöcker, M. Methanol-to-hydrocarbons: catalytic materials and their behavior. *Micropor. Mesopor. Mater.* **29**, 3–48 (1999).
13. Tian, P., Wei, Y., Ye, M. & Liu, Z. Methanol to olefins (MTO): from fundamentals to commercialization. *ACS Catal.* **5**, 1922–1938 (2015).
14. Khodakov, A. Y., Chu, W. & Fongarland, P. Advances in the development of novel cobalt Fischer−Tropsch catalysts for synthesis of long-chain hydrocarbons and clean fuels. *Chem. Rev.* **107**, 1692–1744 (2007).
15. Dry, M. E. The Fischer–Tropsch process: 1950–2000. *Catal. Today* **71**, 227–241 (2002).
16. White, J. L. et al. Light-driven heterogeneous reduction of carbon dioxide: photocatalysts and photoelectrodes. *Chem. Rev.* **115**, 12888–12935 (2015).
17. Surdhar, P. S., Mezyk, S. P. & Armstrong, D. A. Reduction potential of the carboxyl radical anion in aqueous solutions. *J. Phys. Chem.* **93**, 3360–3363 (1989).
18. Hisatomi, T., Kubota, J. & Domen, K. Recent advances in semiconductors for photocatalytic and photoelectrochemical water splitting. *Chem. Soc. Rev.* **43**, 7520–7535 (2014).
19. Morris, A. J., McGibbon, R. T. & Bocarsly, A. B. Electrocatalytic carbon dioxide activation: the rate-determining step of pyridinium-catalyzed CO_2 reduction. *ChemSusChem* **4**, 191–196 (2011).
20. Iizuka, K., Wato, T., Miseki, Y., Saito, K. & Kudo, A. Photocatalytic reduction of carbon dioxide over Ag cocatalyst-loaded $ALa_4Ti_4O_{15}$ (A = Ca, Sr, and Ba) using water as a reducing reagent. *J. Am. Chem. Soc.* **133**, 20863–20868 (2011).
21. Nakanishi, H., Iizuka, K., Takayama, T., Iwase, A. & Kudo, A. Highly active $NaTaO_3$-based photocatalysts for CO_2 reduction to form CO using water as the electron donor. *ChemSusChem* **10**, 112–118 (2017).
22. Yoshida, H. et al. Calcium titanate photocatalyst prepared by a flux method for reduction of carbon dioxide with water. *Catal. Today* **251**, 132–139 (2015).
23. Huang, Z., Teramura, K., Hosokawa, S. & Tanaka, T. Fabrication of well-shaped $Sr_2KTa_5O_{15}$ nanorods with a tetragonal tungsten bronze structure by a flux method for artificial photosynthesis. *Appl. Catal. B* **199**, 272–281 (2016).
24. Pang, R., Teramura, K., Asakura, H., Hosokawa, S. & Tanaka, T. Highly selective photocatalytic conversion of CO_2 by water over Ag-loaded $SrNb_2O_6$ nanorods. *Appl. Catal. B* **218**, 770–778 (2017).
25. Bhugun, I., Lexa, D. & Savéant, J.-M. Catalysis of the electrochemical reduction of carbon dioxide by iron (0) porphyrins. Synergistic effect of Lewis acid cations. *J. Phys. Chem.* **100**, 19981–19985 (1996).
26. Meng, X. et al. Photocatalytic CO_2 conversion over alkali modified TiO_2 without loading noble metal cocatalyst. *Chem. Commun.* **50**, 11517–11519 (2014).
27. Liao, Y. et al. Efficient CO_2 capture and photoreduction by amine-functionalized TiO_2. *Chem. Eur. J.* **20**, 10220–10222 (2014).
28. Huang, Z., Teramura, K., Asakura, H., Hosokawa, S. & Tanaka, T. CO_2 capture, storage, and conversion using a praseodymium-modified Ga_2O_3 photocatalyst. *J. Mater. Chem. A* **5**, 19351–19357 (2017).
29. Teramura, K., Tatsumi, H., Wang, Z., Hosokawa, S. & Tanaka, T. Photocatalytic conversion of CO_2 by H_2O over Ag-loaded SrO-modified Ta_2O_5. *Bull. Chem. Soc. Jpn* **88**, 431–437 (2015).
30. Pang, R. et al. Modification of Ga_2O_3 by an Ag–Cr core–shell cocatalyst enhances photocatalytic CO evolution for the conversion of CO_2 by H_2O. *Chem. Commun.* **54**, 1053–1056 (2018).
31. Pang, R., Teramura, K., Asakura, H., Hosokawa, S. & Tanaka, T. Effect of thickness of chromium hydroxide layer on Ag cocatalyst surface for highly selective photocatalytic conversion of CO_2 by H_2O. *ACS Sustain. Chem. Eng.* **7**, 2083–2090 (2018).
32. Ogata, M., Fujimoto, K. & Shinkai, S. Molecular design of calix[4]arene-based extractants which show high Ca^{2+} selectivity. *J. Am. Chem. Soc.* **116**, 4505–4506 (1994).
33. Moriga, T., Kammler, D. R., Mason, T. O., Palmer, G. B. & Poeppelmeier, K. R. Electrical and optical properties of transparent conducting homologous

compounds in the indium–gallium–zinc oxide system. *J. Am. Ceram. Soc.* **82**, 2705–2710 (1999).
34. Tsuneoka, H., Teramura, K., Shishido, T. & Tanaka, T. Adsorbed species of CO_2 and H_2 on Ga_2O_3 for the photocatalytic reduction of CO_2. *J. Phys. Chem. C* **114**, 8892–8898 (2010).
35. Collins, S. E., Baltanás, M. A. & Bonivardi, A. L. An infrared study of the intermediates of methanol synthesis from carbon dioxide over Pd/β-Ga_2O_3. *J. Catal.* **226**, 410–421 (2004).
36. Collins, S. E., Baltanás, M. A. & Bonivardi, A. L. Infrared spectroscopic study of the carbon dioxide adsorption on the surface of Ga_2O_3 polymorphs. *J. Phys. Chem. B* **110**, 5498–5507 (2006).
37. Fukuda, Y. & Tanabe, K. Infrared study of carbon dioxide adsorbed on magnesium and calcium oxides. *Bull. Chem. Soc. Jpn* **46**, 1616–1619 (1973).
38. Philipp, R. & Fujimoto, K. FTIR spectroscopic study of carbon dioxide adsorption/desorption on magnesia/calcium oxide catalysts. *J. Phys. Chem.* **96**, 9035–9038 (1992).
39. Busca, G. & Lorenzelli, V. Infrared spectroscopic identification of species arising from reactive adsorption of carbon oxides on metal oxide surfaces. *Mater. Chem.* **7**, 89–126 (1982).
40. Tsyganenko, A. & Filimonov, V. Infrared spectra of surface hydroxyl groups and crystalline structure of oxides. *J. Mol. Struct.* **19**, 579–589 (1973).
41. Busca, G., Lamotte, J., Lavalley, J. C. & Lorenzelli, V. FT-IR study of the adsorption and transformation of formaldehyde on oxide surfaces. *J. Am. Chem. Soc.* **109**, 5197–5202 (1987).
42. Wenig, R. W. & Schrader, G. L. In situ FTIR (Fourier transform IR) spectroscopy of 1-butene and 1, 3-butadiene. Selective oxidation to maleic anhydride on vanadium-phosphorus-oxygen catalysts. *J. Phys. Chem.* **91**, 1911–1918 (1987).
43. Teramura, K. et al. Which is an intermediate species for photocatalytic conversion of CO_2 by H_2O as the electron donor: CO_2 molecule, carbonic acid, bicarbonate, or carbonate ions? *J. Phys. Chem. C* **121**, 8711–8721 (2017).
44. Yoshizawa, S. et al. Important role of strontium atom on the surface of $Sr_2KTa_5O_{15}$ with a tetragonal tungsten bronze structure to improve adsorption of CO_2 for photocatalytic conversion of CO_2 by H_2O. *ACS Appl. Mater. Interfaces* **11**, 37875–37884 (2019).
45. Habisreutinger, S. N., Schmidt-Mende, L. & Stolarczyk, J. K. Photocatalytic reduction of CO_2 on TiO_2 and other semiconductors. *Angew. Chem. Int. Ed.* **52**, 7372–7408 (2013).
46. Pang, R., Teramura, K., Asakura, H., Hosokawa, S. & Tanaka, T. Effect of Cr species on photocatalytic stability during the conversion of CO_2 by H_2O. *J. Phys. Chem. C* **123**, 2894–2899 (2019).
47. Sakata, Y., Hayashi, T., Yasunaga, R., Yanaga, N. & Imamura, H. Remarkably high apparent quantum yield of the overall photocatalytic H_2O splitting achieved by utilizing Zn ion added Ga_2O_3 prepared using dilute $CaCl_2$ solution. *Chem. Commun.* **51**, 12935–12938 (2015).

Acknowledgements

This study was partially supported by a Grant-in-Aid for Scientific Research on Innovative Areas, "All Nippon Artificial Photosynthesis Project for Living Earth" [grant number 2406] of the Ministry of Education, Culture, Sports, Science, and Technology (MEXT) of Japan and the Program for Element Strategy Initiative for Catalysts & Batteries (ESICB) [No. JPMXP0112101003], commissioned by the MEXT of Japan.

Author contributions

R.P. and K.T. designed the research. R.P. prepared the photocatalyst powder and conducted XRD, BET, XPS, SEM, TEM, ICP-OES, UV–Vis, and FTIR studies, electrochemical measurements, and the photocatalytic CO_2-conversion experiments. M.M. carried out the isotopic labeling experiment. R.P., K.T., M.M., H.A., S.H., and T.T. discussed the results. R.P. and K.T. wrote the manuscript with contributions from the other authors.

Competing interests

The authors declare no competing interests.

Additional information

Supplementary information is available for this paper at https://doi.org/10.1038/s42004-020-00381-2.

Correspondence and requests for materials should be addressed to K.T. or T.T.

Reprints and permission information is available at http://www.nature.com/reprints

Publisher's note Springer Nature remains neutral with regard to jurisdictional claims in published maps and institutional affiliations.